Contents lists available at ScienceDirect

Carbon

journal homepage: http://ees.elsevier.com

High graphene permeability for room temperature silicon deposition: The role of defects

F. Ronci [a], S. Colonna [a], R. Flammini [a], M. De Crescenzi [b], M. Scarselli [b], M. Salvato [b], I. Berbezier [c], F. Jardali [d], C. Lechner [d], P. Pochet [e], H. Vach [d], P. Castrucci [b,*]

[a] Istituto di Struttura della Materia, CNR (ISM-CNR), 00133, Roma, Italy
[b] Dipartimento di Fisica, Università degli Studi di Roma "Tor Vergata", 00133, Roma, Italy
[c] CNRS, Aix-Marseille Université, IM2NP, UMR 7334, Campus de St. Jérome, 13397, Marseille, France
[d] LPICM, CNRS, Ecole Polytechnique, IPParis, 91128, Palaiseau, France
[e] Department of Physics, IRIG, Univ. Grenoble Alpes and CEA, F-38000, Grenoble, France

ARTICLE INFO

Article history:
Received 17 September 2019
Received in revised form 8 November 2019
Accepted 11 November 2019
Available online xxx

ABSTRACT

Graphene (Gr) is known to be an excellent barrier preventing atoms and molecules to diffuse through it. This is due to the carbon atom arrangement in a two-dimensional (2D) honeycomb structure with a very small lattice parameter forming an electron cloud that prevents atoms and molecules crossing. Nonetheless at high annealing temperatures, intercalation of atoms through graphene occurs, opening the path for formation of vertical heterojunctions constituted of two-dimensional layers. In this paper, we report on the ability of silicon atoms to penetrate the graphene network, fully epitaxially grown on a Ni(111) surface, even at room temperature. Our scanning tunneling microscopy (STM) experiments show that the presence of defects like vacancies and dislocations in the graphene lattice favor the Si atoms intercalation, forming two-dimensional, flat and disordered islands below the Gr layer. *Ab-initio* molecular dynamics calculations confirm that Gr defects are necessary for Si intercalation at room temperature and show that: i) a hypothetical intercalated silicene layer cannot be stable for more than 8 ps and ii) the corresponding Si atoms completely lose their in-plane order, resulting in a random planar distribution, and form strong covalent bonds with Ni atoms.

1. Introduction

Among the high number of exceptional properties, graphene (Gr) has been explored as an ideal blocking layer for atom and molecule diffusion through it [1,2]. Indeed, the combination of its in-plane (σ) and out-of-plane (π) chemical bonds and its small lattice parameter gives rise to a high density of electronic states, leaving a very small hole in the center of the honeycomb structure, and to a repelling field normal to the surface. Theoretical studies reported that the activation energy for the penetration process of light and heavy atoms through a defect-free graphene layer amounts to several eV, hindering the possibility that such a process might occur even at high temperatures [1–4]. In particular, first-principle Density Functional Theory (DFT) calculations displayed that the energy barrier for the penetration process of a Si atom through a defect-free graphene layer is about 3 eV [5]. Even considering the so-called "hot adatom" or "hot precursor" mechanism [6–10], which takes into account the energy released by the adsorption process of the impinging atom in the evaluation of the process energetics, the total energy would still be too small for Si to penetrate an intact graphene layer. Indeed, the adsorption energy of a Si atom impinging on the graphene surface is calculated to range from about 0.8 eV to about 1.7 eV [11–14]. Nonetheless, Si has been reported to experimentally intercalate below graphene, grown or deposited on different substrates, upon annealing at temperatures higher than about 700 K [5,15–20]. At such temperatures, the thermal energy would still be too small (about 0.06 eV) for the intercalation process to occur on defect-free graphene. However, it is well known that actual graphene layers are always characterized by the presence of defects, either point defects in the honeycomb lattice or linear defects at grain boundaries and substrate terrace edges [21–23]. Such defects are expected to strongly reduce the penetration energy barrier, permitting Si atom intercalation beneath graphene [24].

Concerning the chemical nature of the intercalated silicon, several papers report the formation of metal silicides after silicon deposition and annealing on graphene supported on metallic substrates, [5,16–20,24,25] while others describe the possible formation of silicene [12,26–28].

In this paper, we present a comparative study of silicon deposition on two different substrates, namely Gr/Ni(111) and pristine Ni(111), highlighting the influence of the graphene layer on Si reactivity to-

* Corresponding author.
E-mail address: paola.castrucci@roma2.infn.it (P. Castrucci)

https://doi.org/10.1016/j.carbon.2019.11.035
0008-6223/

ward the substrate. In particular, by using scanning tunneling microscopy (STM), Auger electron spectroscopy (AES), low energy electron diffraction (LEED), and *ab initio* molecular dynamics simulations (AIMD), we show that the silicon atoms deposited on a Gr/Ni(111) sample kept at room temperature (RT) may undergo several pathways: i) adsorption of isolated adatoms preferentially located at bridge positions on the honeycomb graphene hexagons, ii) formation of disordered two-dimensional (2D) structures beneath the graphene layer, iii) formation of a few three-dimensional (3D) clusters on top of the graphene surface. These results indicate that a considerable fraction of the deposited silicon is able to penetrate below the graphene layer even at temperatures as low as RT, forming 2D islands between graphene and Ni(111). *First-principles* calculations have been performed to study the energetics of the adsorption process of Si adatoms on the Gr layer and to highlight the different pathways through which Si atoms can penetrate the Gr layer and form Si 2D islands at RT.

2. Experimental

Sample preparation was carried out in an UHV chamber with a base pressure below 1×10^{-10} mbar. The Ni(111) substrate was cleaned by several Ar^+ sputtering (T = 950 K, E = 1.0–0.5 keV) and annealing (T = 1125 K) cycles. Single layer graphene was grown by dosing ethylene at 2×10^{-6} mbar into the preparation chamber while keeping the Ni(111) substrate at 875 K for 90 min. Silicon deposition was performed using an electron bombardment source at constant flux rate of about 0.01 nm/min. Source calibration was achieved by using a refrigerated quartz crystal thickness monitor placed at the very same sample position before and after Si deposition. A detailed description of source calibration is reported in Ref. [29]. Silicon coverage will be reported throughout the paper in terms of monolayers (ML), where 1 ML corresponds to 1 Si atom per Ni(111) unit cell and, consequently, to about 0.37 nm of Si equivalent thickness. LEED patterns and Auger spectra were obtained using an Omicron Specta-LEED optics. The AES spectra have been collected as first derivative of the electron yield. Samples were studied by STM using a Low Temperature STM (Omicron LT-STM) housed in a UHV-connected vacuum chamber with a base pressure below 5×10^{-11} mbar. The STM images were acquired at RT using a W tip cleaned by electron bombardment in UHV. The STM scanner was calibrated measuring the clean Ni(111) surface.

3. Calculation methods

Ab initio calculations were performed by using spin-polarized DFT within the generalized gradient approximation including van der Waals corrections as implemented in the Vienna *ab initio* simulation package (VASP) [30,31]. The Perdew–Burke–Ernzerhof [32] with van der Waals-D2 functional [33] was used to describe the exchange-correlation interaction. The core electrons were described by the projector-augmented wave method [34]. In general, the plane-wave basis set was restricted to a cutoff energy of 500 eV and the Brillouin zone was sampled in **k**-space within a Monkhorst-Pack scheme by a 3x3x1 mesh; except for the Si adatom adsorption calculations on freestanding graphene were the energy cutoff was chosen to be 900 eV and a 15x15x1 Monkhorst-Pack mesh was used. The calculations were performed using a (6 × 6) Gr/Ni(111) surface cell with Gr adsorbed in a bridge-top configuration. The vacuum region was chosen to be 2.0 nm. All systems were fully relaxed by a conjugate gradient method until the forces acting on each atom were less than 0.1 eV/nm. The convergence criterion for total energy self-consistent field calculations was chosen to be 10^{-6} eV. The binding energy, E_b, was calculated as $E_b = E(Si) + E(substrate) - E(Si + substrate)$ where E represents the total energy of the optimized system; a positive value for E_b indicates that the adsorption is the result of an exothermic process and is, therefore, energetically favorable. *Ab initio* molecular dynamics simulations within the NVT ensemble [35] using the Nose-Hoover thermostat [36 for temperature control were performed using VASP. The time step for all AIMD simulation was 1.0 fs.

4. Results and discussion

Fig. 1(a–c) shows the STM images of the Ni(111) substrate after graphene growth at different resolution levels. The 500×500 nm^2 large-scale STM image in (a) displays several Ni(111) steps fully covered by the graphene. One of these steps is zoomed in (b), where a seemingly continuous graphene layer covers the Ni surface terraces and the step. It must be noted that high-resolution STM images of graphene grown on Ni(111) exhibit a hexagonal arrangement rather than the expected honeycomb structure. Indeed, when graphene is grown with the Ni(111) substrate kept at 875 K, a single layer epitaxial growth is observed, with the two C atoms of the two sub-lattices located at inequivalent sites of the substrate surface [23,37–42]. The epitaxial growth occurs thanks to the quite small 0.8% lattice mismatch between the unit cell parameters of graphene ($a = 0.246$ nm) and of Ni(111) ($a = 0.248$ nm) and to the significant interaction between the substrate and graphene. Such a strong interaction, caused by the hybridization of the metal 3d states with the graphene π orbitals, is demonstrated by the absence of Dirac cones in Angular Resolved Photo-Electron Spectroscopy (ARPES) measurements and by the suppression of the typical Raman signal of graphene [38]. Therefore, in order to observe the honeycomb lattice of graphene, a very low bias voltage and a high tunneling current must be used in STM measurements, as shown by the high-resolution STM image in panel (c). The corresponding LEED pattern, reported in Fig. 1(e), displays no difference with respect to the pattern recorded on the Ni(111) substrate before graphene growth (not shown). This evidence proves the epitaxial growth of the graphene layer and the consequent absence of moiré fringes [43,44]. Furthermore, the absence of arched extra spots in Fig. 1(e) demonstrates that a negligible amount, if any, of rotated domains is formed [45].

Fig. 1(d) reports the comparison between the Auger spectra recorded on the sample before and after the RT evaporation of 1.0 ML of Si on Gr/Ni(111). In the Auger spectrum of the pristine Gr/Ni(111) sample, a typical line shape of graphitic carbon interacting with the metal substrate appears. This is demonstrated by the small feature located at a kinetic energy of about 280 eV (see the inset of Fig. 1(d)) which is absent in the case of pure graphene layers [46]. No oxygen contamination within the resolution of our Auger electron spectroscopy measurement is detected (absence of O KVV Auger peak around 510 eV). After Si deposition, the AES spectrum retains the same features for Ni and C, except for the expected intensity decrease of the Ni peak due to the deposited Si. The minima of the first derivative of the Ni $M_{2,3}VV$ and Si $L_{2,3}VV$ Auger features are located, as expected, around at 60 eV and 92 eV, respectively. The LEED pattern after 1 ML Si deposition, reported in Fig. 1(f) and highlighted by red arrows, displays the same spots at hexagon vertexes as in (e), with a significant diffuse background. No further reconstruction or superstructure is detectable, meaning that no crystalline species such as silicon carbide, nickel silicide, silicon 3D islands, or 2D sheets with sizes greater than the coherence length of the LEED technique are formed.

Fig. 2 reports the STM images for the 1 ML Si/Gr/Ni(111) sample, showing that upon Si deposition different features are observed at the surface. In particular, the 50×20 nm^2 STM image in panel (a) shows: bright structures decorating the terrace edges, small islands or clusters with lateral dimension smaller than 10 nm and bright point-like features. The first two kinds of structures, appear in different areas of the surface, will be discussed in the following while here we focus on the point-like features. These are imaged at atomic resolution in Fig. 2(b): four defects are clearly observed in this image, whose size and apparent height, see the line profile in panel (c), suggest that they are Si adatoms adsorbed on top of the graphene layer. The superposition of a honeycomb lattice representing the Gr layer on the STM image demon-

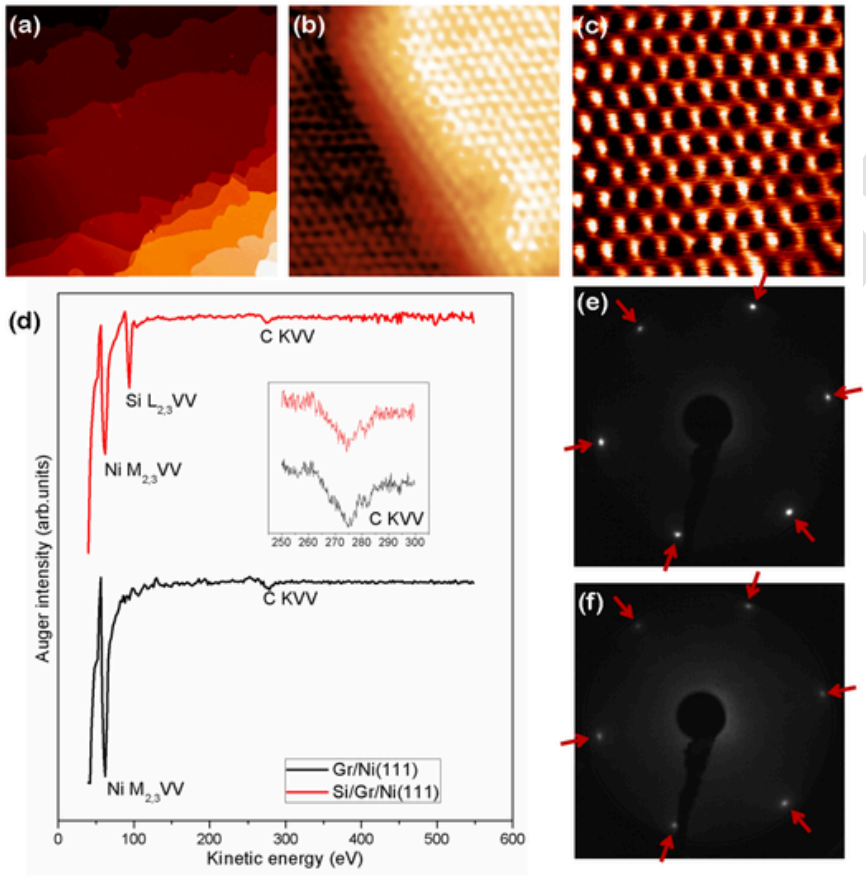

Fig. 1. - Panels (a–c): STM images of the Gr/Ni(111) sample. (a): 500 × 500 nm^2, 100 mV, 5 nA; (b) 5 × 5 nm^2 20 mV, 50 nA; (c) 2.5 × 2.5 nm^2, 5 mV, 100 nA. Panel (d): AES spectra of the graphene/Ni(111) sample before and after 1 ML Si deposition at RT; the C KVV peak is reported at higher energy resolution in the inset for the two curves. Panels (e–f): LEED patterns of the Gr/Ni(111) sample before (e) and after (f) 1ML Si deposition at RT. Red arrows indicate the position of the Gr/Ni(111) substrate spots. (A colour version of this figure can be viewed online.)

strates that all four observed adatoms are located in bridge positions. It must be noted that there are three different bridge positions, placed on top of the three 60°-rotated C–C bonds of Gr, as schematically illustrated in Fig. 2(d) as B1, B2 and B3. Interestingly, given the already discussed inequivalence of the two C atoms in the Gr unit cell, the STM image of such adatoms is consequently asymmetric. Such asymmetry clearly consents the identification of the four adatoms in panel (b): three of them are adsorbed at B1 position and one at B2.

Our STM results are in accordance with theoretical predictions reported in the literature, indicating that the minimum energy position at 0 K for Si atoms adsorbed on a freestanding graphene layer is the bridge position [11,14]. However, Aktürk et al. predict, at temperatures higher than 0 K, Si adatom migration among their calculated bridge, top, and hollow sites [14], which we cannot confirm from our present observations performed at RT. In order to understand our experimental results and to investigate whether the Ni substrate could play a role due to its strong interaction with the graphene layer, we performed *ab-initio* calculations for the three possible positions of a Si atom on both freestanding Gr and Gr/Ni(111) substrates. In the former case, we found a pretty good accordance with the results reported by Akturk et al. [14], obtaining that the bridge position is about 85 meV and 660 meV more stable than the top and the hollow configurations, respectively (see Table 1). Then, we employed the same method for the Gr/Ni(111) system, modeling it with the graphene layer adsorbed in a bridge-top configuration, which is the most stable Gr/Ni(111) adsorption geometry according to our calculations in accordance with recent literature results [40–42]. Interestingly, the presence of the Ni(111) substrate increases the number of inequivalent sites. Indeed, considering a single hexagon in the graphene layer, there is only one hollow position, but there are *a priori* six possible top and bridge configurations. A comparison of the total energy calculations of Si adatom adsorbed at different sites on Gr/Ni(111) confirms that the bridge positions are more stable than the others (see Table 1). Out of the six possible bridge positions, two of them are about 150 meV more stable than the four others. This numerical result confirms what should be expected from symmetry arguments applied to a single surface unit cell, schematically depicted in panel (c) of Table 1: the two preferred configurations are related to the bridge positions above C–C bonds placed on top of a Ni atom (B′ position), while the other four correspond to the two energetically equivalent B″ positions. The six calculated top positions are actually related to the two inequivalent T′ and T″ positions, which are separated by roughly 50 meV. Close inspection of the unique hollow position for the Si adatom shows that the energy difference between the hollow and the bridge positions is more than twice than the one calculated for freestanding graphene, while the energy difference between top and bridge positions increases by a factor 13 relative to the freestanding case (see Table 1). Therefore, these findings demonstrate that, due to the presence of the Ni(111) substrate underneath Gr, the probability for Si adatoms to locate only in bridge configurations at RT is dramatically increased, and in line with our STM measurements. Furthermore, these theoretical results justify the result reported in Fig. 1(c), showing that Si adatoms preferentially adsorb at B1 bridge sites.

Fig. 3(a) reports a 100 × 100 nm^2 STM image displaying the formation of clusters upon Si deposition at RT. These clusters appear ran-

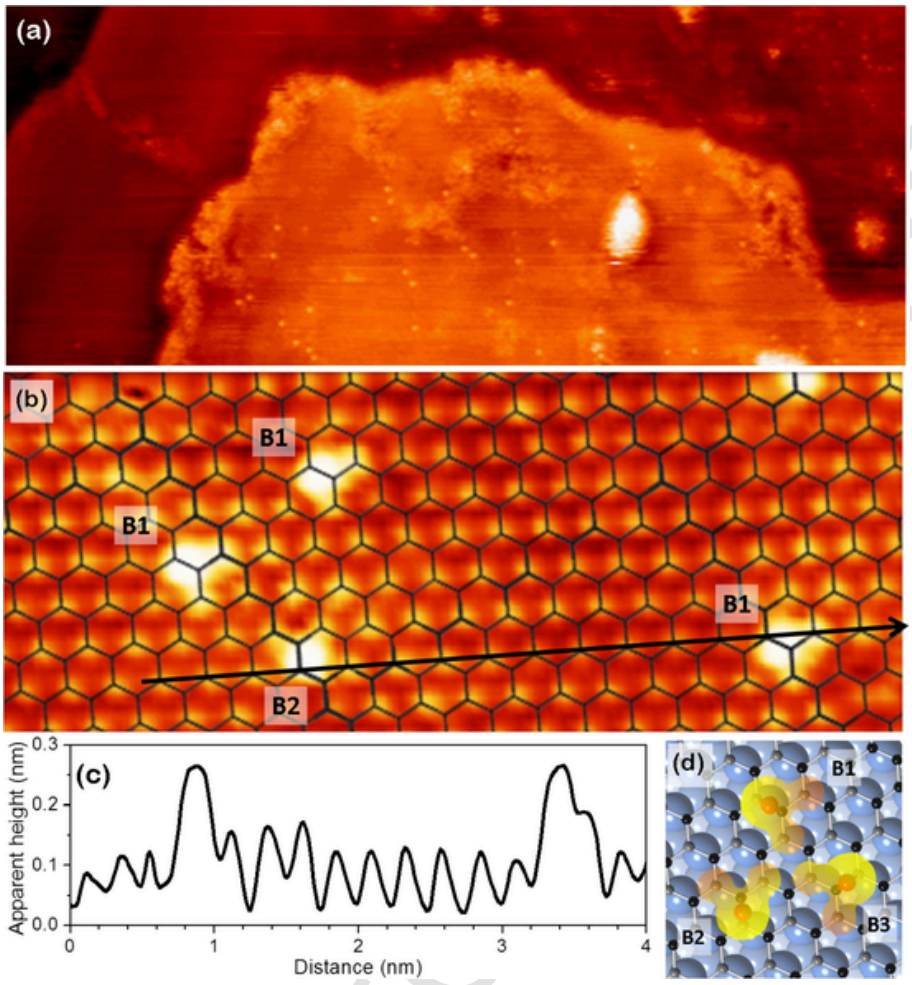

Fig. 2. Panels (a–b): STM images of the 1 ML Si/Gr/Ni(111) sample. (a): 50 × 20 nm^2, 20 mV, 50 nA; (b) 5 × 2 nm^2, 10 mV, 50 nA. Panel (c): Line profile along the black arrow in (b). Panel (d): ball-and-stick model of the Gr layer adsorbed on Ni(111) in a top-bridge configuration: three B1, B2 and B3 bridge adsorption sites for Si adatoms (orange) on graphene (black and gray for the two inequivalent Gr sublattices, black atoms corresponding to bright atoms in graphene STM images) grown on Ni(111) (blue). (A colour version of this figure can be viewed online.)

domly distributed on the Gr/Ni(111) terraces and on the step edges. More importantly, the line profile (in Fig. 3(b) shows that they have almost the same height, ranging from 0.1 to 0.3 nm. Fig. 3(c) reports an atomic resolution STM image of the region highlighted by the upper green rectangle in Fig. 3(a), containing two of these clusters on the surface terrace. The periodicity observed on the clusters is exactly the same as the one of graphene, as demonstrated by the peak distance (0.24 nm) in the line profile shown in Fig. 3(d) and by the two-dimensional fast Fourier transform (2D-FFT) reported in Fig. 3(e). In addition, these islands appear to be almost flat at their top over a distance of a few nanometers and rounded at the border. Fig. 3(f) displays a zoomed-in STM image of the area highlighted by the lower yellow rectangle in panel (a), showing an island located at the step edges with characteristics of flatness, height (see line profile in Fig. 3(g)) and graphene network similar to those exhibited by the islands grown on the terraces. All these findings suggest that Si atoms intercalate through the graphene layer, detaching it from the Ni substrate and forming 2D islands underneath. Interestingly, the graphene layer covering the Ni(111) substrate presents a number of linear and point defects (e.g. dislocations and vacancies) both around the border of the 2D islands and in the pristine Gr layer. Some of these inherent Gr defects are shown by the white arrows in Fig. 3(c). Even though the most part of the bright features appears to have the above discussed characteristics, other features can also be observed on the Gr/Ni(111) surface after the 1.0 ML Si deposition at RT. In the following, we go deeper in the analysis of all these bright features.

Fig. 4(a) displays an atomic resolution STM image of the sample near a terrace edge. In this case, three typical features are visible, highlighted by the black squares and numbered as 1, 2 and 3. The 2D-FFT in panel (c), related to the area contained in the black squares 1 and 2 (hereafter named Inset 1 and 2, respectively), shows six spots located at a hexagon vertexes, typical of a graphene network. Conversely, the 2D-FFT (panel (b)) of the area contained in the black square 3 (hereafter referred as Inset 3), in addition to the spots related to the graphene overlayer, clearly shows inner diffuse $\sqrt{3} \times \sqrt{3}(R30°)$ spots.

In Fig. 4(d), we report the STM image of Fig. 4(a) after applying a low-pass FFT filtering with a threshold indicated by the white circles in panels (b) and (c), i.e. excluding the outer spots in the FFT. It is possible to note in Fig. 4(d) that, after filtering out the graphene periodicity, other features appear in specific areas, particularly, but not exclusively, in the brighter areas of the image in panel (a). In order to better visualize such features, we report in the lower six panels of Fig. 4 the high-pass (HP, top) and low-pass (LP, bottom) FFT filtered images of the three 5 × 5 nm^2 insets of panel (a), using as threshold the white circles in (b) or (c). In this way, the graphene overlayer is imaged in the three top images and the residual low-frequency periodicity in the three bottom panels.

Table 1
Summary of relative energies associated with the different Si adatom sites on top of freestanding graphene and on top of graphene deposited on a Ni(111) substrate; the energy values are given relative to the most stable bridge position. The two upper models highlight the calculated adsorption positions in (a) freestanding Gr and (b) Gr/Ni(111). In (c) the different bridge, top and hollow adsorption sites expected from symmetry arguments in the surface unit cell are reported.

Freestanding Gr	
Si atom position	**Energy [meV]**
Bridge (B)	0
Hollow (H)	660
Top (T)	85
Gr/Ni(111)	
Si atom position	**Energy [meV]**
Bridge (B1 ≡ B′)	0
Bridge (B2 ≡ B″)	150
Bridge (B3 ≡ B″)	149
Bridge (B4 ≡ B′)	3
Bridge (B5 ≡ B″)	150
Bridge (B6 ≡ B″)	149

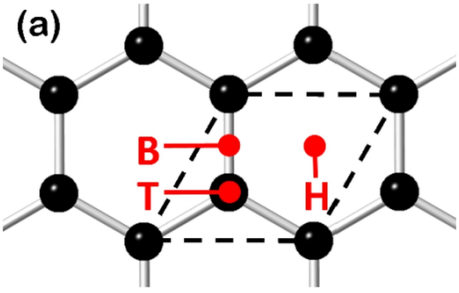

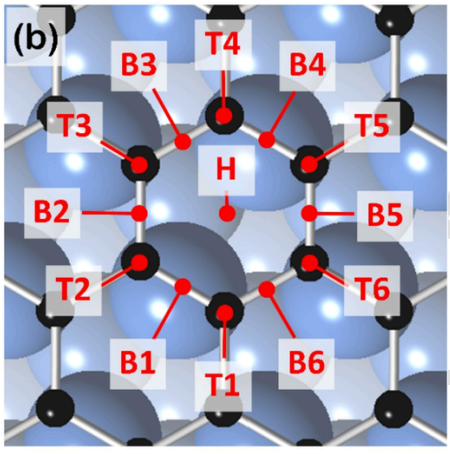

Table 1 (*Continued*)

Freestanding Gr	
Hollow (H)	1768
Top (T1 ≡ T′)	1058
Top (T2 ≡ T″)	1115
Top (T3 ≡ T′)	1058
Top (T4 ≡ T″)	1112
Top (T5 ≡ T′)	1059
Top (T6 ≡ T″)	1115

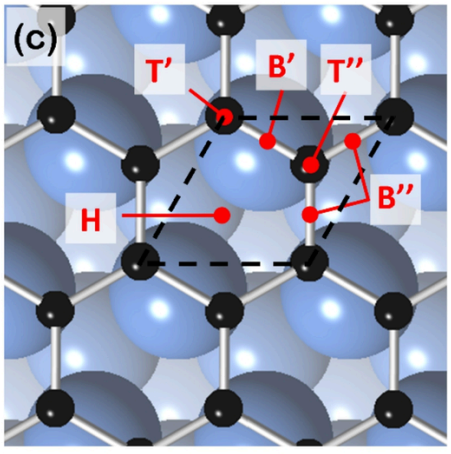

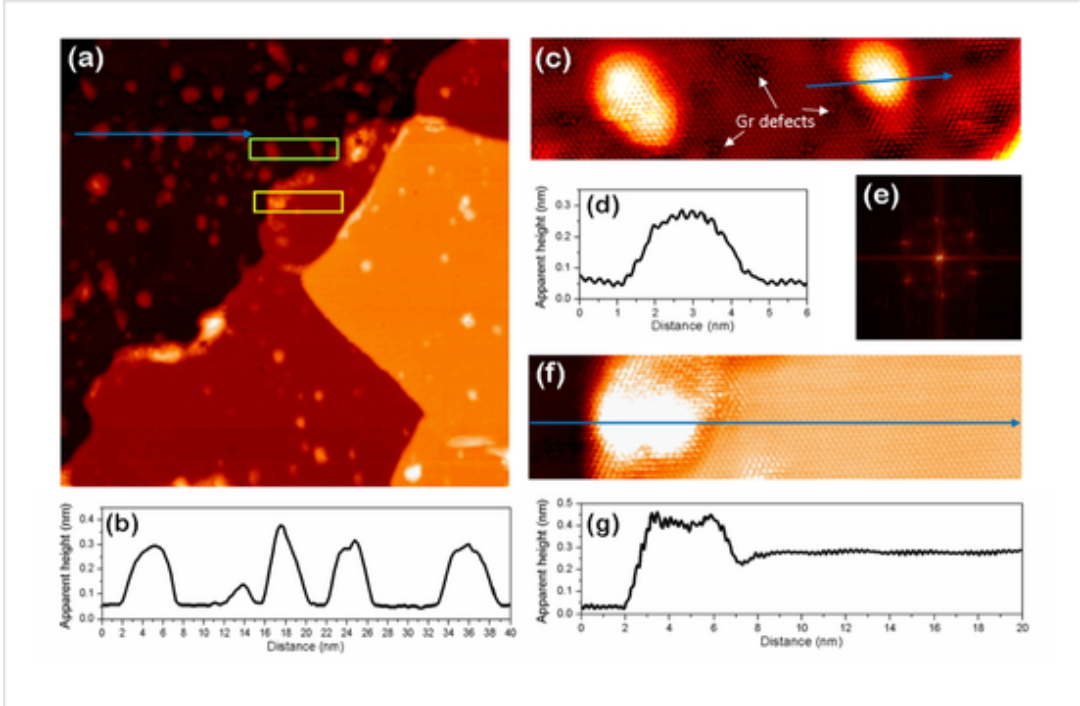

Fig. 3. Panel (a): 100 × 100 nm^2 STM image of the 1 ML Si/Gr/Ni(111) sample (100 nA, 20 mV) and related line profile (b). Panel (c): blow up of the area on the surface terrace highlighted in panel (a) with a green rectangle, line profile (d) and 2D-FFT of the island on the right (e). Note the white arrows highlighting the presence of defects both around the 2D islands and on the pristine Gr layer. Panel (f): blow up of the area at the step edge highlighted in panel (a) with a yellow rectangle and a related line profile (g). (A colour version of this figure can be viewed online.)

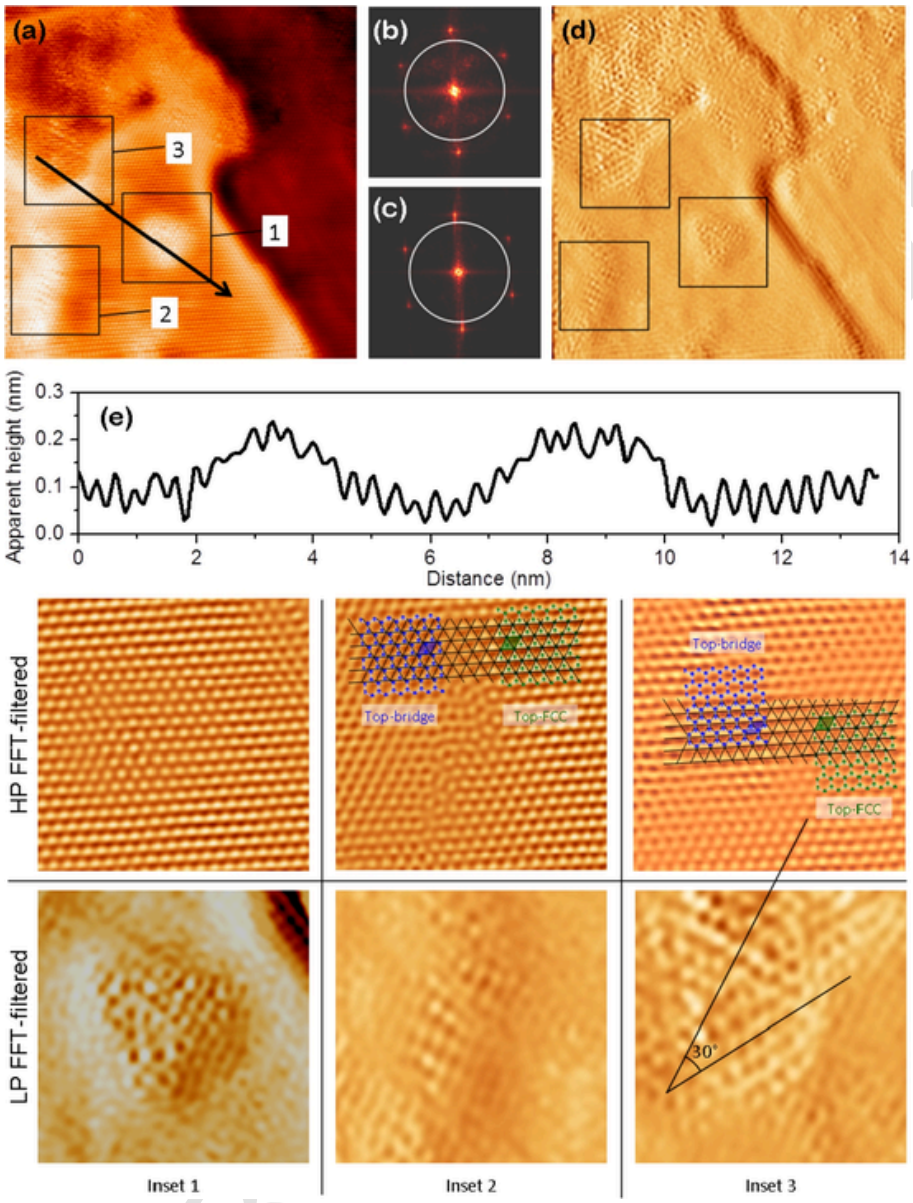

Fig. 4. - Panel (a): $20 \times 20\,nm^2$ STM image of the 1 ML Si/Gr/Ni(111) sample (10 mV, 100 nA). Panel (b): 2D-FFT of area 3 in panel (a). Panel (c): 2D-FFT of area 1 and 2 in panel (a). Panel (d): STM image reported in (a) after applying a low-pass (FFT filter with threshold highlighted by a white circle in (b) and (c). Panel (e): line profile taken along the arrow in (a). Lower panels: high-pass (HP, top) and low-pass (LP, bottom) FFT-filtered $5 \times 5\,nm^2$ images of the insets labeled 1, 2 and 3 in (a). A derivative filter along the x axis was applied on LP FFT-filtered images for better visibility, See text for discussion. (A colour version of this figure can be viewed online.)

We consider Inset 1 first, characterized by the presence of a small island. The line profile reported in Fig. 4(e) shows, as already discussed above, that the island top is almost flat within about 2 nm, with an apparent height of about 0.2 nm. Notably, the HP image of the same area shows a continuous hexagonal periodicity of the graphene overlayer, with a barely visible local distortion at the island location, confirming that the island is formed underneath a continuous graphene layer. After filtering out the graphene periodicity, see the relative LP image, an apparently disordered modulation is observed in correspondence of the island in the central part of the image. The same procedure was performed on the area in Inset 2, characterized by the presence of a bright elongated feature: in this case, a disordered structure with a height of about 0.2 nm emerges in the LP image, separating two apparently different Gr areas, as clearly visible in the HP image. This structure again suggests the formation of a disordered island under the graphene overlayer. A clear difference between the left and the right part of the HP image is observed: the Gr layer is imaged with a honeycomb lattice on the left and a hexagonal pattern on the right. This evidence can be explained taking into account that the epitaxial Gr layer may grow on Ni(111) assuming different adsorption configurations, namely top-hcp, top-fcc and top-bridge [38]. Our calculations confirm that the top-bridge configuration is the most stable one, but the top-fcc is only 6 meV/atom less stable. This means that different adsorption geometries coexist at the Gr/Ni(111) surface and, consequently, that linear defects are necessarily formed at domain borders between adjacent Gr domains with different adsorption configuration [23,38,41]. In this specific case, a domain boundary between top-bridge (left) and top-fcc (right) is formed, as highlighted by the ball and stick model superposed on the HP-FFT filtered STM image. In this model the top-fcc and top-bridge adsorption geometries are reported, along with the relative lozenges representing their unit cells, in green and blue colors, respectively. The black lines, representing the hexagonal lattice of the topmost Ni layer, clearly show the relative in-plane shift between

the two Gr domains. It is worth noting that the right part of Inset 2 displays the same domain as in Inset 1, see Fig. 4(a); hence, the Gr layer in Inset 1 is adsorbed on Ni(111) with a top-fcc configuration.

We like to point out that, as shown further on, our AIMD calculations quantitatively confirm the experimental observation of an intercalated silicon island. Without any intercalated silicon atoms, we find an average distance between the nickel substrate and the Gr layer of about 0.20 nm at room temperature, in accordance with [47]. With 1 ML of intercalated silicon, this distance increases to about 0.44 nm showing that the Gr layer became detached from the nickel substrate and moved upwards by about 0.24 nm, which is in excellent agreement to the experimental finding displayed in Fig. 4(e).

Moving the attention to Inset 3, the relative HP image reveals, similarly to Inset 2, the presence of both a honeycomb (upper-left part) and a hexagonal (lower-right part) appearance of the Gr layer, suggesting the presence of a similar domain boundary, as highlighted by the superposed model. Once again, the top-fcc configuration of the lower-right part confirms the top-fcc adsorption configuration of the Gr layer in Inset 1. Interestingly, in this case the LP image clearly shows a $\sqrt{3} \times \sqrt{3}(R30°)$ periodicity in the upper-left area, in agreement with the 2D-FFT pattern reported in panel (b). In addition, there is no apparent height difference between the $\sqrt{3} \times \sqrt{3}(R30°)$ region and the surrounding graphene areas, as visible in the line profile reported in Fig. 4(e). This evidence will be discussed further on in the text.

The results so far reported suggest that the deposited silicon atoms may follow different pathways at RT, namely (a) adsorb as single adatoms at bridge sites on the graphene lattice, and (b) intercalate below the graphene layer. In addition, we also observed some three-dimensional clusters (STM images not shown here) on the Gr layer, as also reported in Refs. [5,18,24,26]. This observation of high graphene permeability was quite surprising at first sight since silicon intercalation through graphene is generally reported to occur only at significantly higher temperatures, i.e. above about 700 K [5,15,16,48]. The possibility that the impinging silicon atoms may penetrate a defect-free graphene layer must be ruled out since the calculated energy barrier for such a process is of the order of 3 eV. [5] Even taking into account the "hot adatom" or "hot precursor" concept [6–10], which considers that the energy E_{ads}(Si) released upon silicon adsorption on the graphene layer may play a role on the possible processes accessible to the Si adatoms immediately after adsorption, the total Si adatom energy would be too small for the penetration process to occur at RT. In fact, E_{ads}(Si) is calculated to range from about 0.8 eV [11] to about 1.7 eV [13], a much smaller value than the activation energy barrier for the penetration process. However, it is possible that, in the presence of defects in the graphene overlayer, Si atoms may intercalate with a significantly reduced activation energy barrier [24]. Indeed, intercalation of Si atoms deposited on a Gr/Ni(111) sample was already suggested in the literature to partially occur at RT on the basis of core level spectroscopy results [25]. Moreover, as shown in Fig. 3(c) and in Fig. 4-Inset 2, STM images detected defects on the Gr layer at the border or underneath the Si 2D intercalated islands, respectively. Hence, in the following section we consider the possibility that a fraction of the deposited silicon atoms may intercalate at specific defect sites (vacancies, dislocations, boundary domains and step edges) of the graphene layer even at RT.

In order to go deeper into the intercalation mechanism for the Si/Gr/Ni(111) system, we performed a number of theoretical calculations to evaluate the possible role of the so-called "hot precursor" mechanism. To this end, we calculated the adsorption energy of Si atoms at the different adsorption sites (bridge, top, hollow) for both a freestanding Gr layer and for the Gr/Ni(111) substrate (see Table 2). For the bridge site on freestanding Gr layer, our results are in perfect agreement with previously published values [11]. It can be noted that the adsorption energy values significantly increase in the presence of Ni(111), but yet their values are not sufficiently high for allowing Si penetration through a defect-free Gr layer, a process whose energy barrier is about 3 eV [5].

Table 2
Summary of binding energies E_b associated with the different Si adatom adsorption sites on top of freestanding graphene and on top of graphene deposited on a Ni(111) substrate.

Si atom position	E_b [eV] for Gr	E_b [eV] for Gr/Ni(111)
Bridge	0.7922	2.2784
Hollow	0.1319	0.5108
Top	0.7067	1.2194

We then considered the possible effect of the presence of defects in the Gr layer on Si intercalation, investigating the interaction of Si atoms with single, double, triple and larger vacancies at the Gr layer (called V1, V2, V3 for the removal of one, two, or three C-atoms and C6 for the removal of an entire C-hexagon). In all cases, we demonstrate that an incoming thermalized Si atom has the tendency to "repair" the hole, either substituting the missing carbon atoms or getting covalently bond above the defect. Running a large number of MD trajectories with various impact energies, we could then evaluate the energy barrier for Si penetration through such defects and obtained a much reduced value of about 0.5 eV, *i.e.* still about 20 times the thermal energy at RT. It is then clear that even in this situation thermalized Si adatoms cannot penetrate such a barrier directly. However, impinging Si atoms that first adsorb at the Gr are able to penetrate such defects, exploiting the excess energy released upon adsorption. Indeed, in all cases, the absorption energy, ranging from about 0.5 to 2.3 eV, is above the 0.5 eV penetration barrier, thus allowing Si atom intercalation through graphene defects due to a hot precursor mechanism. In summary, the amount of intercalated Si atoms at RT is limited to a quite small fraction and intercalation may occur only at Gr defects, such as vacancies, dislocations, domain boundaries or terrace steps. These theoretical findings are consistent with our experimental STM images, showing the presence of rare and small Si intercalated areas, mostly at Ni terrace edges and Gr domain boundaries where the probability to find defects in the graphene layer is much higher. On the other hand, impinging Si atoms that do not adsorb at or near Gr defects rapidly reach thermal equilibrium with the substrate, dissipating the adsorption energy through other channels; e.g. phonon coupling and/or adatom diffusion, and finally forming 3D Si clusters or remaining adsorbed as isolated adatoms on top of the Gr layer bridge sites.

The results reported in Fig. 4 can now be interpreted in the light of silicon intercalation at Gr defects: the disordered features observed in the LP-FFT images in Fig. 4 can be attributed to the formation of Si structures beneath the Gr layer formed upon Si intercalation through Gr defects. In the case of the area in Inset 1, we observe that a small island is formed beneath an apparently defect-free Gr layer, according to the relative HP-FFT image. Hence, we infer that Si intercalation occurred through point defects in the Gr layer, possibly removed through a self-healing process as suggested in Refs. [24,49]. Another hypothesis is that the island could have been formed by an in-plane diffusion process of the Si atoms after intercalation through the defects at the very close step edge. In the sample areas highlighted in Insets 2 and 3, conversely, in-plane 1D structures are observed protruding from the surface in Fig. 4(a). The relative LP-FFT images suggest that Si intercalation, in these cases, occurred through Gr defects at the domain boundaries that are clearly observed in the related HP-FFT images. Concerning the nature of such structures, we can speculate that the intercalated silicon atoms should react with the substrate to form different kinds of nickel silicides, as demonstrated to occur when silicon is deposited directly on Ni(111) at RT [50]. In our case, however, silicon is deposited on top of a graphene layer and not directly on the

Ni(111) substrate, resulting, in a reduced Si/Ni reactivity since Si atoms necessarily lose a large part, if not all, of their initial absorption energy upon intercalation through the defect. Hence, we considered the possibility that silicon may form a low interacting silicene layer between Gr and Ni(111). To explore such a possibility, we have modeled a perfect nickel/silicene/graphene sandwich and we performed molecular dynamics calculations to evaluate the stability and/or the evolution of the silicene layer underneath Gr at finite temperatures. To this end, we carefully heated the "sandwich" up to room temperature and let the system evolve at the target temperature for 8 ps. No intermixing between Si and Ni atoms is observed during this simulation time at 300 K. However, although they remain sandwiched between Gr and Ni(111) in a bidimensional layer, the Si atoms completely lose their in-plane order resulting in a random planar distribution and form strongly interacting covalent bonds with Ni atoms (see Fig. 5) that reduce their in-plane mobility considerably. This theoretical result is in perfect agreement with the STM image, 2D-FFT, and the line profile displayed in Fig. 4 and in Fig. 3(c). In order to observe intermixing (alloy formation), within the simulation period, the sample temperature must be increased at least to 475 K according to our AIMD simulations.

We will now focus our attention on the origin of the $\sqrt{3}\times\sqrt{3}(R30°)$ periodicity observed in the reciprocal space pattern in Fig. 4(b) and, in real space in the LP-FFT filtered STM image of Inset 3 in Fig. 4. Such a periodicity may be ascribed i) to the formation of ordered nickel silicide; ii) to the formation of an ordered silicon 2D honeycomb layer, e.g. silicene, on top of Gr/Ni(111) or iii) to the intervalley scattering phenomenon.

As for case i), the formation of ordered $\sqrt{3}\times\sqrt{3}(R30°)$ Ni_2Si was already observed upon silicon deposition on a clean Ni(111) surface and subsequent annealing above 600 K [42]. Our molecular dynamics calculations confirm that heating to at least 475 K is required to have Ni–Si alloy formation within an 8 ps time lapse. It is obviously possible that, due to the very short time period considered, small patches of ordered $\sqrt{3}\times\sqrt{3}(R30°)$ nickel silicide may form after longer simulation times. However, this hypothesis is in contradiction with the results reported for Si deposition at RT on Gr/Ni(111), [25] reporting no hint of ordered silicide phases formed after Si deposition at RT. On the other hand, in case ii) we consider the possibility that the $\sqrt{3}\times\sqrt{3}(R30°)$ periodicity might be the result of the formation of an ordered 2D silicene layer. Indeed, the calculated silicene unit cell parameter, even for a small size silicene nanosheet, is 0.38–0.40 nm [51–53], close to the one of $\sqrt{3}\times\sqrt{3}(R30°)$ graphene (0.42–0.43 nm). However, according to our AIMD simulations, silicon atoms are expected to react with nickel even at RT and to arrange in a disordered network, as discussed above. Furthermore, even assuming that such a reaction was somehow blocked, we should expect an apparent height difference between the $\sqrt{3}\times\sqrt{3}(R30°)$ region and the surrounding area which is not observed in the present case, see the line profile reported in Fig. 4(e). The last hypothesis, case iii), considers intervalley electron backscattering of π-like states. Such a phenomenon has been reported to be the cause for the observed $\sqrt{3}\times\sqrt{3}(R30°)$ modulation in graphene near defects [54,55] or grain boundaries [56]. The peculiarity of intervalley electron backscattering is that the resulting $\sqrt{3}\times\sqrt{3}(R30°)$ periodicity is a direct consequence of the position of the K and K' points in the graphene Brillouin zone [18,57]. Hence, we infer that the observed $\sqrt{3}\times\sqrt{3}(R30°)$ periodicity may be attributed to intervalley scattering of Gr of π-like states.

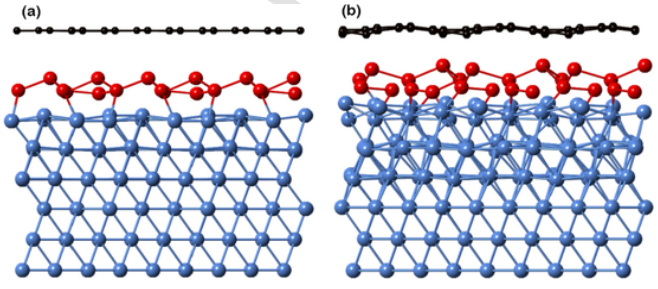

Fig. 5. Side views of the initial optimized Ni(111)/silicene/graphene structure at zero Kelvin (left side) and the same structure at room temperature (right side). (A colour version of this figure can be viewed online.)

Let's finally turn our attention to the role of the graphene layer and its defects. In our case, as in Ref. [25], silicon is deposited on top of a graphene layer and not directly on the Ni(111) substrate, as in Ref. [50]. This difference seems to play an important role on silicon reactivity toward the substrate: we have already discussed that, according to the "hot adatom" model, the impinging Si atoms may exploit the energy released upon adsorption to penetrate through defects in the graphene layer and intercalate below it. At variance with a direct deposition on Ni(111), the Si atoms react with the substrate with a much reduced energy since the fraction of Si atoms that reach the Ni surface has already dissipated part of its adsorption energy to penetrate the Gr layer. Furthermore, in the presence of the Gr layer, Si atoms react with nickel only at Gr defects, with a consequent localized deposition and reduced Si–Ni reactivity with respect to a direct Si deposition on Ni(111). This is, indeed, proved by comparing Fig. 6(a) and (b), reporting the STM images of 1 ML Si deposited at RT on Ni(111) and on Gr/Ni(111), respectively. It can be noted that in the former case the deposited silicon is distributed all over the surface and forms islands involving one or two atomic layers reaching heights up to 0.4–0.5 nm (see line profile in Fig. 6(c)). Instead, in the Gr/Ni(111) case, as already discussed above, Si atoms aggregate in clusters with a height between 0.1 and 0.3 nm underneath the graphene overlayer (Fig. 6(d)), leaving large graphene areas uncovered. In both cases, LEED measurements (see Fig. 6(e and f)) exhibit no extra spots, but in the former case, the LEED pattern shows a much higher diffuse background and less clear bulk spots with respect to the latter, demonstrating the formation of a highly disordered surface coating (see Fig. 6(a)), rather than the formation of 2D islands, as observed in Fig. 6(b). This is consistent with the results reported in ref. [50], where from x-ray photoelectron spectroscopy a model of the Si–Ni(111) interface has been suggested to form a rough surface due to the interdiffusion of Si atoms in the Ni matrix giving rise to an intermetallic compound ordered at short distance.

5. Conclusions

In summary, we have studied Si deposition at room temperature on a graphene monolayer epitaxially grown on a Ni(111) substrate. We have found a significant permeability of the graphene layer that allows Si intercalation at room temperature. The presence of Gr domain boundaries and/or C atom vacancies in the graphene layer permits the penetration of the impinging Si atoms through the Gr sheet, giving rise mainly to the formation of two-dimensional flat islands. These islands are disordered, nanometric in size with an apparent height of about 0.2 nm and are able to detach the Gr overlayer from the Ni(111) substrate. Theoretical calculations show that the high impermeability of graphene is, indeed, considerably lowered by the presence of defects on the Gr layer, allowing the intercalation of deposited Si atoms even at room temperature and leading to the formation of two-dimensional intercalated and disordered Si islands interacting with the Ni substrate. Such strong interaction prevents the formation of ordered two-dimensional silicon structures (e.g. silicene) beneath the graphene layer. The reported method, however, can be a route to form vertical heterojunctions at room temperature and could be envisaged as a viable route to silicene formation, provided a substrate with lower reactivity toward silicon is selected. Finally, the comparative study of the Si/Ni interaction with and without a graphene layer demonstrates that its presence plays an important role, limiting the amount and the energy of sili-

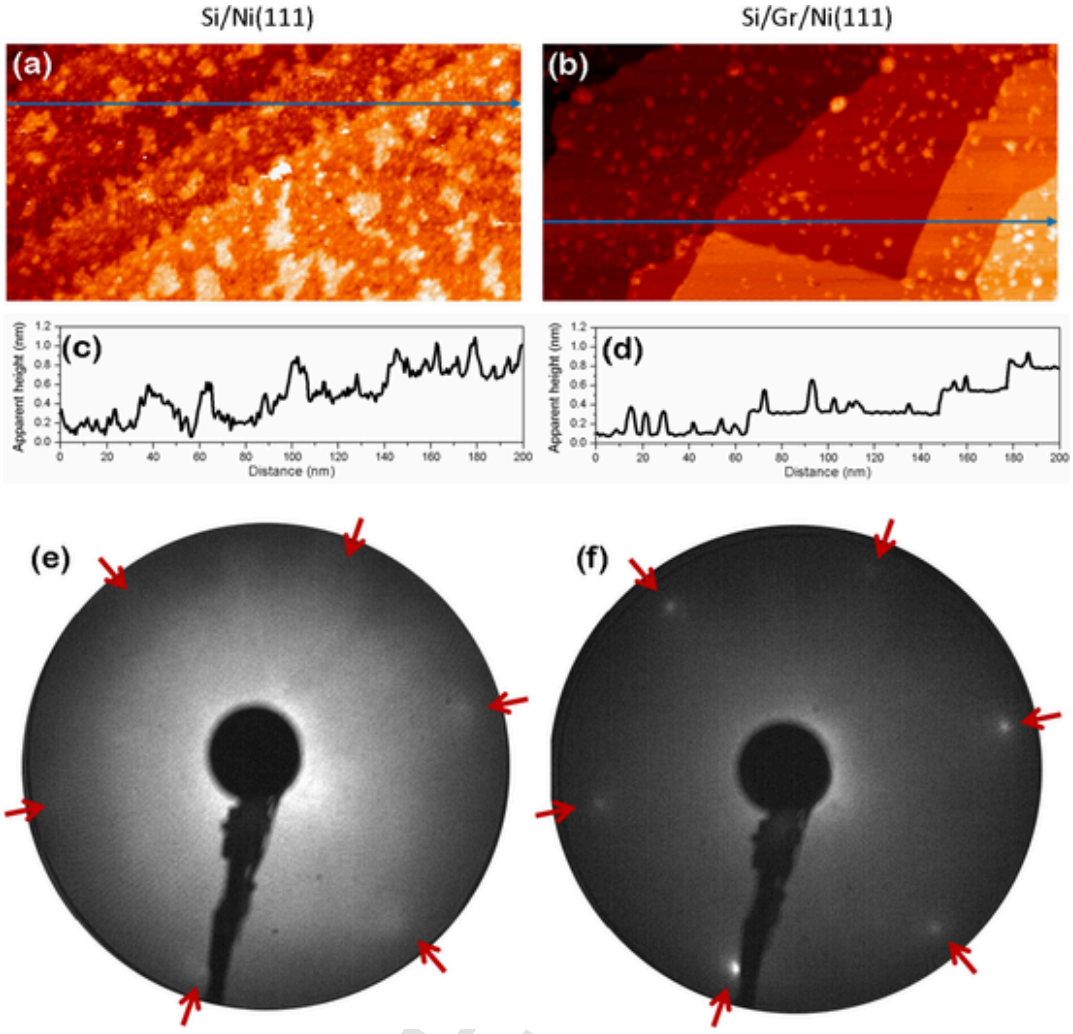

Fig. 6. STM images of 1 ML Si deposition at RT on (a) Ni(111) (200 × 100 nm^2, 0.1 V, 5 nA) and (b) Gr/Ni(111) (200 × 100 nm^2, 0.02 V, 100 nA). Panels (c) and (d): Line profiles taken along the blue lines in (a) and (b), respectively. Panels (e) and (f): Corresponding LEED patterns. Red arrows indicate the position of the faint substrate bulk spots. (A colour version of this figure can be viewed online.)

con atoms that react with nickel, preventing the formation of 3D alloy clusters.

Declaration of competing interest

The authors declare that they have no known competing financial interests or personal relationships that could have appeared to influence the work reported in this paper.

Acknowledgements

We would like to warmly thank Mauro Satta for helpful discussion and feedback. P.C., M. D.C., M.S and M.S. would like to acknowledge the European Community for the HORIZON2020 MSC-RISE Project DiSeT-Com (GA 823728). H.V., F.J., and C.L. gratefully acknowledge the HPC centers of the IDRIS (Grant A004-0900642) and CERMM for computational resources and the Hariri Foundation for Sustainable Human Development for the scholarship awarded to F.J..

P.P. acknowledges GENCI for computational resources (GENCI-6194 at the CINES super-computing center).

References

[1] V. Berry, Impermeability of graphene and its applications, Carbon 62 (2013) 1–10.

[2] L. Tsetseris, S.T. Pantelides, Graphene: an impermeable or selectively permeable membrane for atomic species?, Carbon 67 (2014) 58–63.

[3] J. Sun, S. Li, T. Stirner, J. Chen, D. Wang, Molecular dynamics simulation of energy exchanges during hydrogen collision with graphite sheets, J. Appl. Phys. 107 (2010) 113533.

[4] E. Despiau-Pujo, A. Davydova, G. Cunge, L. Delfour, L. Magaud, D.B. Graves, Elementary processes of H2 plasma-graphene interaction: a combined molecular dynamics and density functional theory study, J. Appl. Phys. 113 (2013) 114302.

[5] Y. Cui, J. Gao, L. Jin, J. Zhao, D. Tan, Q. Fu, et al., An exchange intercalation mechanism for the formation of a two-dimensional Si structure underneath graphene, Nano Res 5 (2012) 352–360.

[6] J. Harris, B. Kasemo, On precursor mechanisms for surface reactions, Surf. Sci. 105 (1981) L281–L287.

[7] J. Barth, Transport of adsorbates at metal surfaces: from thermal migration to hot precursors, Surf. Sci. Rep. 40 (2000) 75–149.

[8] H. Nienhaus, Electronic excitations by chemical reactions on metal surfaces, Surf. Sci. Rep. 45 (2002) 1–78.

[9] J. Meyer, K. Reuter, Modeling heat dissipation at the nanoscale: an embedding approach for chemical reaction dynamics on metal surfaces, Angew. Chem. Int. Ed. 53 (2014) 4721–4724.

[10] M. Satta, S. Colonna, R. Flammini, A. Cricenti, F. Ronci, Silicon reactivity at the Ag(111) surface, Phys. Rev. Lett. 115 (2015) 026102.

[11] V.O. Özçelik, D. Kecik, E. Dorgun, S. Ciraci, Adsorption of group IV elements on graphene, silicene, germanene, and Stanene: Dumbbell formation, J. Phys. Chem. C 119 (2015) 845–853.

[12] G.R. Berdiyorov, M. Neek-Amal, F.M. Peeters, A.C.T. van Duin, Stabilized silicene within bilayer graphene: a proposal based on molecular dynamics and density-functional tight-binding calculations, Phys. Rev. B 89 (2014) 024107.

[13] A. Ishii, M. Yamamoto, H. Asano, K. Fujiwara, DFT calculation for adatom adsorption on graphene sheet as a prototype of carbon nano tube functionalization, J. Phys. Conf. Ser. 100 (2008) 052087.

[14] E. Aktürk, C. Ataca, S. Ciraci, Effects of silicon and germanium adsorbed on graphene, Appl. Phys. Lett. 96 (2010) 123112.
[15] C. Xia, S. Watcharinyanon, A.A. Zakharov, R. Yakimova, L. Hultman, I. Johansson, et al., Si intercalation/deintercalation of graphene on 6H-SiC(0001), Phys. Rev. B 85 (2012) 045418.
[16] S. Lizzit, R. Larciprete, P. Lacovig, M. Dalmiglio, F. Orlando, A. Baraldi, et al., Transfer-free electrical insulation of epitaxial graphene from its metal substrate, Nano Lett. 12 (2012) 4503–4507.
[17] L. Meng, R. Wu, H. Zhou, G. Li, Y. Zhang, L. Li, et al., Silicon intercalation at the interface of graphene and Ir(111), Appl. Phys. Lett. 100 (2012) 083101.
[18] J. Mao, L. Huang, Y. Pan, M. Gao, J. He, H. Zhou, et al., Silicon layer intercalation of centimeter-scale, epitaxially grown monolayer graphene on Ru(0001), Appl. Phys. Lett. 100 (2012) 093101.
[19] M.G. Silly, M. D'Angelo, A. Besson, Y.J. Dappe, S. Kubsky, G. Li, et al., Electronic and structural properties of graphene-based metal-semiconducting heterostructures engineered by silicon intercalation, Carbon 76 (2014) 27–39.
[20] R. Larciprete, P. Lacovig, F. Orlando, M. Dalmiglio, L. Omiciuolo, A. Baraldi, et al., Chemical gating of epitaxial graphene through ultrathin oxide layers, Nanoscale 7 (2015) 12650–12658.
[21] F. Banhart, J. Kotakoski, A.V. Krasheninnikov, Structural defects in graphene, ACS Nano 5 (2011) 26–41.
[22] P. Jacobson, B. Stöger, A. Garhofer, G.S. Parkinson, M. Schmid, R. Caudillo, et al., Disorder and defect healing in graphene on Ni(111), J. Phys. Chem. Lett. 3 (2012) 136–139.
[23] J. Lahiri, P. Bozkurt, Oleynik, M. Batzill, An extended defect in graphene as a metallic wire, Nat. Nanotechnol. 5 (2010) 326–329.
[24] G. Li, H. Zhou, L. Pan, Y. Zhang, L. Huang, W. Xu, et al., Role of cooperative interactions in the intercalation of heteroatoms between graphene and a metal substrate, J. Am. Chem. Soc. 137 (2015) 7099–7103.
[25] O. Vilkov, A. Fedorov, D. Usachov, L.V. Yashina, A.V. Generalov, K. Borygina, et al., Controlled assembly of graphene-capped nickel, cobalt and iron silicides, Sci. Rep. 3 (2013) 2168.
[26] M. De Crescenzi, I. Berbezier, M. Scarselli, P. Castrucci, M. Abbarchi, A. Ronda, et al., formation of silicene nanosheets on graphite, ACS Nano 10 (2016) 11163–11171.
[27] R. van Bremen, Q. Yao, S. Banerjee, D. Cakir, N. Oncel, H.J.W. Zandvliet, Intercalation of Si between MoS_2 layers, Beilstein J. Nanotechnol. 8 (2017) 1952–1960.
[28] M. Neek-Amal, A. Sadeghi, G.R. Berdiyorov, F.M. Peeters, Realization of free-standing silicene using bilayer graphene, Appl. Phys. Lett. 103 (2013) 261904.
[29] C. Hogan, S. Colonna, R. Flammini, A. Cricenti, F. Ronci, Structure and stability of Si/Ag(110) nanoribbons, Phys. Rev. B 92 (2015) 115439.
[30] G. Kresse, J. Furthmu¨ller, Efficiency of ab initio total energy calculations for metals and semiconductors using a plane-wave basis set, Comput. Mater. Sci. 6 (1996) 15–50.
[31] G. Kresse, J. Furthmüller, Efficient iterative schemes for ab initio total-energy calculations using a plane-wave basis set, Phys. Rev. B 54 (1996) 11169–11186.
[32] J.P. Perdew, K. Burke, M. Ernzerhof, Generalized gradient approximation made simple, Phys. Rev. Lett. 77 (1996) 3865–3868.
[33] S. Grimme, Semiempirical GGA-type density functional constructed with a long-range dispersion correction, J. Comput. Chem. 27 (2006) 1787–1799.
[34] P.E. Blöchl, Projector augmented-wave method, Phys. Rev. B 50 (1994) 17953–17979.
[35] R. Windiks, B. Delley, Massive thermostating in isothermal density functional molecular dynamics simulations, J. Chem. Phys. 119 (2003) 2481–2487.
[36] S.A. Nosé, Unified formulation of the constant temperature molecular-dynamics methods, J. Chem. Phys. 81 (1984) 511–519.
[37] Y. Gamo, A. Nagashima, M. Wakabayashi, M. Terai, C. Oshima, Atomic structure of monolayer graphite formed on Ni(111), Surf. Sci. 374 (1997) 61–64.
[38] A. Dahal, M. Batzill, Graphene–nickel interfaces: a review, Nanoscale 6 (2014) 2548–2562.
[39] J. Lahiri, T.S. Miller, A.J. Ross, L. Adamska, Oleynik, M. Batzill, Graphene growth and stability at nickel surfaces, New J. Phys. 13 (2011) 025001.
[40] W. Zhao, S.M. Kozlov, H. Höfert, K. Gotterbarm, M.P.A. Lorenz, F. Viñes, et al., Graphene on Ni(111): coexistence of different surface structures, J. Phys. Chem. Lett. 2 (2011) 759–764.
[41] F. Bianchini, L.L. Patera, M. Peressi, C. Africh, G. Comelli, Atomic scale identification of coexisting graphene structures on Ni(111), J. Phys. Chem. Lett. 5 (2014) 467–473.
[42] S.C. Matysik, C. Papp, A. Görling, Solving the puzzle of the coexistence of different adsorption geometries of graphene on Ni(111), J. Phys. Chem. C 122 (2018) 26105–26110.
[43] T. Iwasaki, H.J. Park, M. Konuma, D.S. Lee, J.H. Smet, U. Starke, Long-range ordered single-crystal graphene on high-quality heteroepitaxial Ni thin films grown on MgO(111), Nano Lett. 11 (2011) 79–84.
[44] R. Rosei, M. De Crescenzi, F. Sette, C. Quaresima, A. Savoia, P. Perfetti, Structure of graphitic carbon on Ni(111): a surface extended energy loss structure study, Phys. Rev. B 28 (1983) 1161–1164.
[45] L.L. Patera, C. Africh, R.S. Weatherup, R. Blume, S. Bhardwaj, C. Castellarin-Cudia, et al., In situ observations of the atomistic mechanisms of Ni catalyzed low temperature graphene growth, ACS Nano 9 (2013) 7901–7912.
[46] M. Xu, D. Fujita, J. Gao, N. Hanagata, Auger electron spectroscopy: a rational method for determining thickness of graphene films, ACS Nano 4 (2010) 2937–2945.
[47] G. Bertoni, L. Calmels, A. Altibelli, V. Serin, First-principles calculation of the electronic structure and EELS spectra at the graphene/Ni(111) interface, Phys. Rev. B 71 (2004) 075402.
[48] L. Meng, R. Wu, H. Zhou, G. Li, Y. Zhang, L. Li, et al., Silicon intercalation at the interface of graphene and Ir(111), Appl. Phys. Lett. 100 (2012) 083101.
[49] V.O. Özçelik, H.H. Gurel, S. Ciraci, Self-healing of vacancy defects in single-layer graphene and silicene, Phys. Rev. B 88 (2013) 045440.
[50] B. Lalmi, C. Girardeaux, A. Portavoce, C. Ottaviani, B. Aufray, J. Bernardini, Formation and stability of a two-dimensional nickel silicide on Ni(111): an Auger, LEED, STM, and high-resolution photoemission study, Phys. Rev. B 85 (2012) 245306.
[51] S. Cahangirov, M. Topsakal, E. Aktürk, H. Sahin, S. Ciraci, Two- and one-dimensional honeycomb structures of silicon and germanium, Phys. Rev. Lett. 102 (2009) 236804.
[52] L. Matthes, O. Pulci, F. Bechstedt, Massive Dirac quasiparticles in the optical absorbance of graphene, silicene, germanene, and tinene, J. Phys. Condens. Matter 25 (2013) 395305.
[53] P. Castrucci, F. Fabbri, T. Delise, M. Scarselli, M. Salvato, S. Pascale, et al., Raman investigation of air-stable silicene nanosheets on an inert graphite surface, Nano Res 11 (2018) 5879–5889.
[54] G.M. Rutter, J.N. Crain, N.P. Guisinger, T. Li, P.N. First, J.A. Stroscio, Scattering and interference in epitaxial graphene, Science 317 (2007) 219–222.
[55] L. Tapasztó, G. Dobrik, P. Nemes-Incze, G. Vertesy, P. Lambin, L.P. Biró, Tuning the electronic structure of graphene by ion irradiation, Phys. Rev. B 78 (2008) 233407.
[56] J. Tian, H. Cao, W. Wu, Q. Yu, Y.P. Chen, Direct imaging of graphene edges: atomic structure and electronic scattering, Nano Lett. 11 (2011) 3663–3668.
[57] W. Peng, T. Xu, P. Diener, L. Biadala, M. Berthe, X. Pi, et al., Resolving the controversial existence of silicene and germanene nanosheets grown on graphite, ACS Nano 12 (2018) 4754–4760.